Title

Stress relaxation in pre-stressed aluminum core–shell particles: X-ray diffraction study, modeling, and improved reactivity

Authors

Levitas, Valery I
McCollum, Jena
Pantoya, Michelle L
et al.

Publication Date

2016-08-01

DOI

10.1016/j.combustflame.2016.05.012

Peer reviewed

Stress relaxation in pre-stressed aluminum core-shell particles: *In situ* x-ray diffraction study, modeling, and improved reactivity

Commented [PM1]: Valery – shouldn't this be Synchrotron and not In situ?

Commented [LV[E2R1]: Please ask Nobumichi, It looks fine to me

Valery I. Levitas[1], Jena McCollum[2], Michelle L. Pantoya[2], and Nobumichi Tamura[3]*

[1] *Iowa State University, Department of Aerospace Engineering, Department of Mechanical Engineering, Department of Material Science and Engineering, Ames, Iowa 50011, USA*

[2]*Mechanical Engineering, Texas Tech University, Lubbock, TX 79409, USA*

[3] *Advanced Light Source, Lawrence Berkeley National Laboratory, Berkeley, CA 94720, USA*

*Corresponding author, email: *vlevitas@iastate.edu*

Keywords: aluminum, residual stresses, annealing, stress relaxation, synchrotron XRD , strain, flame propagation speed, reactivity

Abstract

Stress relaxation in aluminum micron-scale particles covered by alumina shell after pre-stressing by thermal treatment and storage was measured using x-ray diffraction with synchrotron radiation. Pre-stressing was produced by annealing Al particles at 573 K followed by fast cooling. While averaged dilatational strain in Al core was negligible for untreated particles, it was measured at 4.40×10^{-5} and 2.85×10^{-5} after 2 and 48 days of storage. Consistently, such a treatment lead to increase in flame propagation speed for Al+CuO mixture by 37% and 25%, respectively. Analytical model for creep in alumna shell and stress relaxation in Al core-alumina shell structure is developed and activation energy and pre-exponential multiplier are estimated. The effect of storage temperature and annealing temperature on the kinetics of stress relaxation

was evaluated theoretically. These results provide estimates for optimizing Al reactivity with the holding time at annealing temperature and allowable time for storage of Al particles for different environmental temperatures.

I. INTRODUCTION

Chemical reaction of aluminum nano- and micron-scale particles with various oxidizers (e.g., MoO_3, Fe_2O_3, and CuO) is of significant practical importance because these reactions exhibit high energy densities and high flame (energy) propagation speeds. Controlling and optimizing Al particle reactivity requires understanding the reaction mechanisms. Different mechanisms operate under different conditions: diffusion mechanism [1-3], reaction sintering [4], and melt-dispersion-mechanism (MDM) [5,6]. Our focus here is on the very high heating rate regimes for which mechanochemical MDM is claimed [5,6]. Initially [5,7], this mechanism was suggested to rationalize extremely high flame speed V (up to 1 km/s) observed for combustion of Al nanoparticles [7-9]. Later [10,11], the MDM was generalized for few-micron-scale Al particles. The main idea of the MDM is that melting of Al core is accompanied by a 6% dilatational strain that generates pressures in the range of 1 to 3 GPa in the molten Al core and tensile hoop stress σ_h in the Al_2O_3 shell higher than the ultimate strength of the Al_2O_3 shell (i.e., ~11.33 GPa). Such stresses overload, fracture, and spallate the alumina shell during high rate heating and straining, because time required for stress relaxation is longer than the loading and fracture time. Disappearance of the shell leads to pressure drop down to almost zero at the bare molten Al surface, while pressure in the bulk of the core remains the same. Such pressure distribution produces an unloading spherical wave moving to the center of the core that generates a tensile mean stress up

to 8 GPa near the core center. High tension disperses the Al melt into small fragments; convective gas flow and collisions of particles facilitate dispersion. Thus, MDM transforms a single Al particle protected by an alumina shell into multiple smaller bare droplets, and their oxidation is not controlled by diffusion through the initial shell.

Numerous confirmations of the MDM, mostly in flame tube experiments [5-7,10-11] but also in flash ignition experiments [12], have been obtained for nano- and micron-scale particles. The chief quantitative confirmation of the MDM consists of reproducing a complex relationship between the normalized flame speed V/V_{max} (i.e., V_{max} is the maximum possible flame speed in the same experimental set-up under the same conditions, i.e., geometry, bulk density of the mixture, stoichiometry, etc.) and the ratio $M=R/\delta$ of the core radius R to the oxide shell thickness δ [5-7,10-11]. Such an analytical quantitative model provides methods to control (increase) particle reactivity and, consequently, the flame speed [5-7,10-11,13,14].

One prediction was that producing initial compressive stress in the alumina shell and, consequently, tensile stress in the Al core suppresses fracture of the oxide during heating and increases V/V_{max} [5,6]. As it follows from the equation for V/V_{max}, initial compressive stress in the shell can be produced by increasing the temperature T_0 at which thermal stresses in the Al core-oxide shell structure are absent. Usually, T_0 is considered room temperature, because either the initial alumina shell was formed at room temperature, or because internal stresses relax with time during particle storage at room temperature. It was suggested in [5] that annealing the core-shell particle structure to a higher temperature, T_a, would lead to relaxation of internal stresses and alter the stress-free temperature T_0 to T_a. Fast quenching rate is required in order to avoid relaxation of new internal stresses that appear during cooling of the particles down to the room temperature. With such an approach for pre-stressing, the temperature T_0 was increased to different values in

the range 378-473 K, which indeed increased flame speed for Al nano- and micron-scale particles by 30-40%, in quantitative agreement with theoretical predictions [13,14].

To conceptually and quantitatively prove that the improvement of Al reactivity is indeed related to internal stresses, the dilatation strains in Al core for micron-scale particles were measured for untreated Al particles and particles annealed at 573K and quenched at 0.46 K/s using x-ray diffraction with synchrotron radiation [15]. Experimental results confirmed theoretical estimates and proved that the improvement of Al reactivity is due to internal stresses.

An important problem that was not considered before is determination of the kinetics of internal stress relaxation. During Al particle storage, internal stresses relax over time and the positive effect from annealing may reduce or disappear. For this reason, typical relaxation times are important to estimate in order to recommend optimal time between heat treatment and usage. Essentially, Al particle reactivity may be enhanced with annealing and quenching, but the enhancements may have an expiration date. Also, kinetics of internal stress relaxation for a given annealing temperature is required to determine the hold time at the annealing temperature. In addition, relaxation of the internal stresses during fast heating in combustion experiments determine critical heating rate for transition from the diffusion mechanism of oxidation to MDM. Our goal here is to study kinetics of stress relaxation in Al micron-size particles at room temperature after annealing and quenching to room temperature and stored for different times. The results are correlated to the flame speed produced by the particles after the same storage time. Also, a continuum model for creep in the alumina shell and stress and strain evolution is developed and main parameters for creep (i.e., activation energy and pre-exponential multiplier) are estimated. This analysis allowed us to theoretically model stress relaxation during annealing as well. Practical recommendations on the admissible time of storage of annealed Al particles at

different environmental temperatures and holding time during annealing at different temperatures are suggested.

II. Experimental

II.1. Sample Preparation

Aluminum particles with a 3.0-4.5 μm particle diameter were procured from Alfa Aesar (Ward Hill, MA) and used for this study. Particle size response to annealing and quenching treatment is characterized in [15,16] showing no significant deviation in average particle diameter with annealing and quenching treatment.

Aluminum particles (200 mg) were loaded into ceramic trays and heated to 573 K at 10 K/min and held for 15 minutes. After heating, the trays were removed from the oven and quenched to room temperature by refrigeration. This process used a Neytech Qex vacuum oven (Torrance, CA) in an air environment. Each thermal cycle was monitored using an InstruNet Direct to Sensor system (Charlestown, MA) and Type K thermocouples from Omega Engineering (Stamford, CT). Aluminum temperature response as a function of time is shown in [1].

Due to natural convection conditions, the Al cooled according to lump capacitance. The temperature evolution reduces exponentially and experimental results are approximated by the following equation:

$$T = T_{am} + (T_a - T_{am}) \exp(-At) \text{ with } A = 0.0078\ s^{-1}$$

Here, T_{am} is ambient temperature, T_a is annealing temperature, t is time and A is determined by examining the exponential plots of the cooling curve and identifying the coefficient. An average quenching rate is 0.38 $K \cdot s^{-1}$ for this thermal treatment.

Post-treatment, Al particles were mixed with 50 nm average particle diameter spherical CuO particles (Sigma Aldrich; St. Louis, MO) to an equivalence ratio of 1.2 (i.e., slightly fuel rich). The mixing process is well documented but will be summarized here. The dry powders were weighed and suspended in hexane as a carrier fluid to aid intermixing, then mixed using a Misonix Sonicator 3000 probe for 2 minutes. The solution was poured into a Pyrex dish and hexane evaporated in a fume hood for 24 hours. The dry powders were retrieved and sieved to break up large agglomerations.

The powder was carefully loaded into 3 mm inner diameter, 8 mm outer diameter, 10 cm long quartz tubes containing 700 mg of powder each. The theoretical maximum density (TMD) of the loose powder is determined by a weighted average of the bulk densities of Al (2.7 $g \cdot cm^{-3}$), Al_2O_3 (3.95 $g \cdot cm^{-3}$), and CuO (6.31 $g \cdot cm^{-3}$) and determined to be 4.91 $g \cdot cm^{-3}$. The measured bulk density is 0.98 $g \cdot cm^{-3}$ such that all tubes were loaded to a constant density of 20% TMD.

II.2. Strain Measurements

X-Ray Diffraction (XRD) experiments were performed at the Advanced Light Source on beamline 12.3.2 using a micron focused synchrotron x-ray beam. We have detailed the use of this instrumentation for strain measurements on thermally treated Al particles in our previous work [15, 16] but the method is summarized here for completeness. Aluminum powder samples were spread over glass slides and scanned under the x-ray beam (either polychromatic or monochromatic) while a diffraction pattern was collected at each step using a DECTRIS Pilatus 1 M detector. The measured relative small shifts in the reflection positions in the Laue pattern provides the deviatoric strain tensor of the material while the measurement of the energy of one reflection provides the dilatational component. Data were processed using XMAS software [17]. The beamline experimental setup and capabilities have been described elsewhere [18].

II.3. Flame Speed Measurements

Figure 1 illustrates a typical powder filled tube arrangement for measuring flame speed as well as representative still frame images of flame propagation. The apparatus and procedure are described in more detail elsewhere [13,14,16,19] but summarized here. Both ends of the tube were sealed with one side securing a length of nickel-chromium wire for ignition. Five experiments per annealing temperature were performed to establish repeatability. Each tube was placed inside a blast chamber for ignition and flame propagation experiments. The powders were ignited and flame propagation was observed through a viewing window in the chamber. The reaction was recorded with a Phantom v7 (Vision Research, Wayne, NJ) high speed camera at a rate of 29,000 frames per second and 512 x 128 resolution. The camera was aligned perpendicular to the direction of flame propagation. Flame speed was determined by tracking the flame front through a referenced time and distance using the Vision Research Software. The resolution of the flame speed for this diagnostic is 0.1 $m \cdot s^{-1}$. The largest source of uncertainty in the measurement is due to repeatability and is shown for each data set in the results.

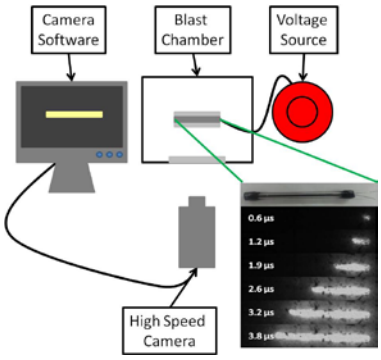

Figure 1. Flame speed apparatus with representative time stamped still frame images of flame speed for an Al-CuO mixture.

II.4. Experimental Results

Figures 2 and 3 show plots for the dilatational strain and average peak width distributions, respectively, from synchrotron XRD measurements. Average strain values were calculated by performing a count weighted average of the distribution shown in Fig. 2. The strain values for the treated Al particles represent the change in volume from the untreated case. Resolution for the instrument is $1x10^{-5}$. Since the measured strain for untreated particles is below this value, it can be considered as zero strain. The strain values for the annealed Al particles aged for 2 days and 48 days are outside this resolution and demonstrate a measureable change. Results for averaged dilatational strain from the current experiments and from [15] are collected in Table 1.

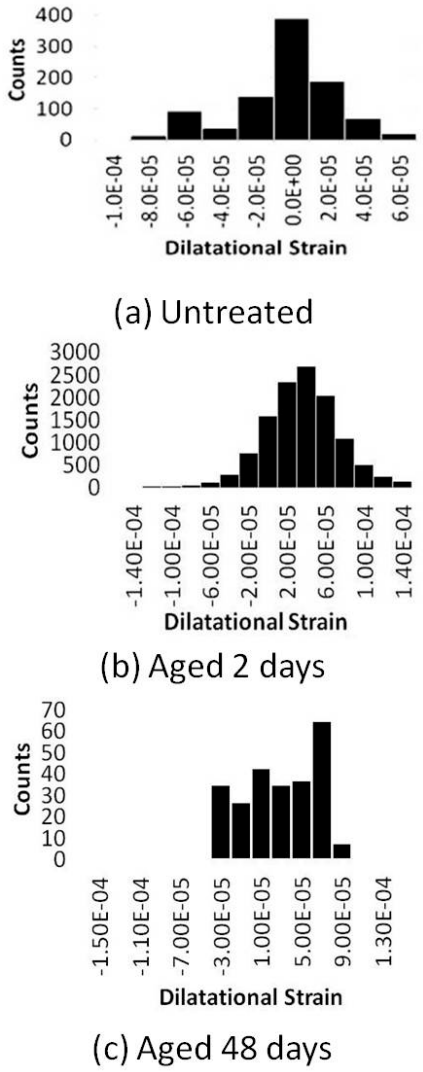

Figure 2. Dilatational strain plots for (a) untreated Al, and Al annealed to 573 K, cooled to room temperature and aged (b) 2 days; and, (c) 48 days.

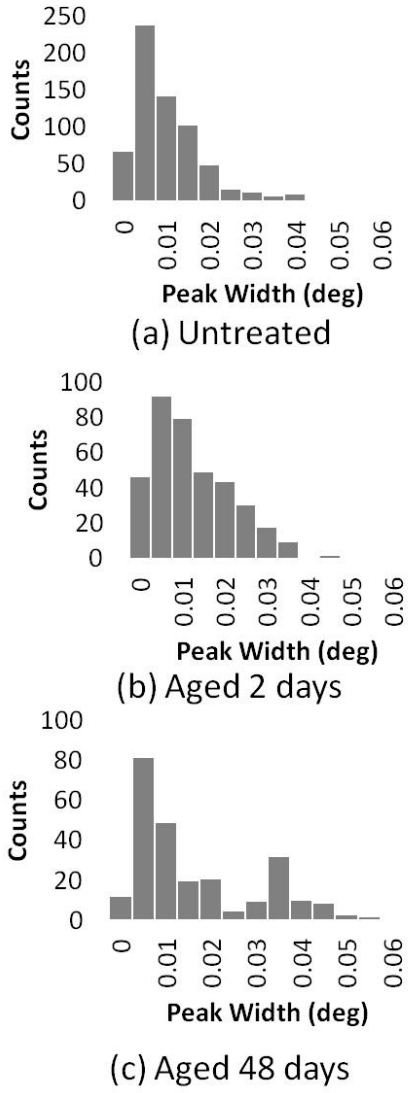

Figure 3. Peak width for (a) untreated Al, and Al annealed to 573 K, cooled to room temperature and aged (b) 2 days; and, (c) 48 days.

Measured flame propagation speed for untreated particles was 95 m/s, after treatment and 2 days aging flame speed increase to 130 m/s, and after 48 days of aging flame speed reduced to 119 m/s. These values are essentially lower than those in [15] due to greater compaction of the powder. Indeed, compaction to 16% TMD in [15] reduced flame speed in comparison with compaction to 8% TMD in [14]. Relative flame speed values for each aged sample are shown in Table 1. The flame speed is normalized to the untreated flame speed such that a percent increase is apparent. Both samples annealed to 573 K show an increase from the untreated case. Treated samples aged for 2 days resulted in a 37% increase and 25% increase for 48 days. These data are consistent with 32% increase in flame rate after similar heat treatment and aging for 46 days [15]. Values for flame speed and averaged dilatational strain are also summarized in Table 1.

Table 1. Dilatational strain values and percent increase in flame speed for all samples.

Sample	Average Strain	Measured Flame Speed m/s	Flame Speed % Increase
Untreated	1.5×10^{-6}	95	---
2 days	4.40×10^{-5}	130	37 ± 2%
48 days	2.85×10^{-5}	119	25 ± 2%

III. Modeling

III.1. Qualitative discussion

There are two types of internal stresses in Al particles: (a) hydrostatic mean stress (pressure) due to interaction between particle and shell and (b) stresses due to heterogeneities in Al, including intergranular internal stresses in polycrystalline aggregate and stresses due to defects generated during plastic relaxation. Our focus is on controlling mean stresses due to interaction between core and shell, which is characterized by temperature T_0 at which core-shell

system is stress-free. Untreated particles have practically zero average dilatational strain, which means that T_0 coincides with the ambient temperature, T_a. Distribution of dilatational strain in Fig. 2a characterizes the hydrostatic part of the second type of stresses due to intergranular heterogeneity. Distribution of the peak width in Fig. 3a characterizes mostly the magnitude and heterogeneity of deviatoric (nonhydrostatic) stresses. Annealing at 573 K relaxes average dilatational strain due to interaction between core and shell thus shifting T_0 to 573 K, and also partially relaxes intergranular stresses. Ideally, fast quenching should not lead to stress relaxation and should generate hydrostatic pressure in the Al core and tensile hoop stress in a shell. In reality, stresses can partially relax during cooling. Fast quenching is required in order to reach low temperature as soon as possible, because the lower temperature is, the smaller relaxation rate. After quenching and 2 days aging, a broad distribution of dilatational strain is observed (Fig. 2b), caused by significant heterogeneity of the intergranular stresses that did not have enough time to relax. Peak width reduced during annealing (Fig. 3b) due to relaxation of deviatoric stresses. After 48 days of aging, dilatational strain partially relaxed, and also lead to its reduced heterogeneity (Fig. 2c). Since relaxation involves not only creep in alumina shell but also some plastic straining in polycrystalline core; such a plastic straining leads to increase in magnitude and heterogeneity of intergranular deviatoric stresses (Fig. 3c).

III.2. Equation for the creep strain rate

We will focus on stress relaxation due to creep in an amorphous alumina shell and neglect intergranular stresses and their relaxation. Since there is no information about creep in few nm thick alumina shell, we will consider the simplest diffusion-controlled creep described by Eq. (1) [Frost HJ, Ashby MF (1989) Deformation-Mechanism Maps (Pergamon Press, New York).].

$$\dot{\boldsymbol{\varepsilon}}_c = \mu \exp\left(-\frac{Q}{kT}\right)\boldsymbol{s}, \qquad (1)$$

In Eq. (1), $\dot{\boldsymbol{\varepsilon}}_c$ is the creep strain rate tensor, $\boldsymbol{s}$ is the deviatoric stress tensor, μ is a proportionality factor, Q is the activation energy, and k= 1.38×10^{-23} J/K is the Boltzmann constant. The alumina shell thickness, δ, is small in comparison with the particle core radius R, nominal $M=R/\delta$ is in the range 500 to 2000, that is why radial dependence of stresses and strains in the shell will be neglected. Based on results in [15] for micron scale particles, the effect of surface energy and stresses can be neglected. Then shell is under biaxial tension produced by hoop stress σ_h with principle stresses (σ_h, σ_h, 0), mean stress $\sigma_m = (\sigma_h + \sigma_h + 0)/3 = 2/3\sigma_h$, and the principle components of the deviatoric stress are (σ_h - σ_m, σ_h - σ_m, 0- σ_m)= (σ_h, σ_h, -2 σ_h)/3. Due to plastic incompressibility, $\varepsilon_c^r + 2\varepsilon_c^h = 0$, where ε_c^r and ε_c^h are the radial and hoop creep strain, the principle components of the creep strain are $(\varepsilon_c^h, \varepsilon_c^h, -2\varepsilon_c^h)$. Then the only independent part of Eq.(1) is the hoop component shown in Eq. (2).

$$\dot{\varepsilon}_c^h = \mu \exp\left(-\frac{Q}{kT}\right)\sigma_h/3 = \bar{\mu}\exp\left(-\frac{Q}{kT}\right)\sigma_h = \tilde{\mu}\sigma_h; \qquad \bar{\mu} = \mu/3; \qquad \tilde{\mu} = \bar{\mu}\exp\left(-\frac{Q}{kT}\right). \quad (2)$$

III.3. Stresses and strain in the core-shell structure

Using traditional methods of solving elastic problem with thermal and creep strains (eigen strains) for elastic core and shell and generalizing our results [5,6] for creep strain, we obtain for the hoop stress in the shell at the boundary with the core, σ_h, described in Eq. (3) and (4).

$$\sigma_h = -\frac{6(m^3+2)(\varepsilon_2^T - \varepsilon_1^T)G_2K_1K_2}{H} - \frac{2\varepsilon_c^h G_2\left(4\left(m^3-1\right)G_2\left(3K_2-K_1\right)+9m^3K_1K_2\right)}{H}; \quad (3)$$

$$\varepsilon_1^T = \alpha_1(T - T_0); \quad \varepsilon_2^T = \alpha_2(T - T_0); \quad m = 1 + 1/M; \quad H = 3m^3K_1K_2 + 4G_2(K_1 + (m^3-1)K_2) \quad (4)$$

Here subscripts 1 and 2 designate Al core and alumina shell, respectively, α is the linear thermal expansion coefficient, G and K are the shear and bulk moduli, and *T* is the particle temperature, which is the room temperature at the instant of strain measurement. The second term due to creep strain in Eq. (3) is the new one, otherwise, this equation is the same as in [5,6]. Expressing σ_h in the form $\sigma_h = B - C\varepsilon_c^h$ with B and C defined from Eq. (3) and substituting it in Eq. (2), we obtain the differential equation for evolution of the creep strain shown in Eq. (5).

$$\dot{\varepsilon}_c^h = \tilde{\mu}(B - C\varepsilon_c^h) \qquad (5)$$

The solution with initial condition $\varepsilon_c^h(0) = 0$ is shown in Eq. (6).

$$\varepsilon_c^h = \frac{B}{C}(1 - \exp(-\tilde{\mu}Ct)) \qquad (6)$$

Next, we can do simplifications similar to those in [9] utilizing that *m-1* is a small number and keeping the linear in *m-1* terms only to produce Eq. (7).

$$\sigma_h = -\frac{18(\varepsilon_2^T - \varepsilon_1^T + \varepsilon_c^h)G_2K_1K_2}{H_s}; \quad H_s = (3K_2 + 4G_2)K_1 \qquad (7)$$

Thus, the creep hoop strain just adds to other eigen strains, namely to the difference in thermal strains in the shell and core. If one cuts a particle in two equal parts and considers equilibrium of one-half-particle, then

$$\sigma_0\pi R^2 + \sigma_h 2\pi R\delta = 0 \quad \Rightarrow \quad \sigma_0 = -\frac{2\sigma_h}{M} = \frac{36(\varepsilon_2^T - \varepsilon_1^T + \varepsilon_c^h)G_2K_1K_2}{MH_s}. \qquad (8)$$

It follows from Eq. (7) that

$$B = -\frac{18(\varepsilon_2^T - \varepsilon_1^T)G_2K_1K_2}{H_s}; \quad C = \frac{18G_2K_1K_2}{H_s}, \quad \text{and} \quad \frac{B}{C} = \varepsilon_1^T - \varepsilon_2^T, \qquad (9)$$

and Eq. (6) simplifies to

$$\varepsilon_c^h = (\varepsilon_1^T - \varepsilon_2^T)(1 - \exp(-\tilde{\mu}Ct)). \quad (10)$$

Then the evolution of the dilatational strain in the core is described in Eq. (11).

$$\varepsilon_0 = \frac{\sigma_0}{K_1} = -\frac{2\sigma_h}{MK_1} = \frac{36(\varepsilon_2^T - \varepsilon_1^T)G_2K_2}{MH_s}\exp(-\tilde{\mu}Ct) = \frac{2(\varepsilon_2^T - \varepsilon_1^T)C}{MK_1}\exp(-\tilde{\mu}Ct). \quad (11)$$

III.4. Parameter identification

Utilizing the same material properties as in [15] (see Table 2), we obtain *C=525.1 GPa* and from Eq. (11),

$$\varepsilon_0 = \frac{2.468\times10^{-4}\left(T_0 - T\right)}{M}\exp(-525.1\tilde{\mu}t). \quad (12)$$

Ratio

$$\frac{\varepsilon_0(2\,\text{days})}{\varepsilon_0(48\,\text{days})} = \frac{\exp(-525.1\tilde{\mu}\times 2)}{\exp(-525.1\tilde{\mu}\times 48)} \quad (13)$$

is independent of T_0 and M and using experimental data from Table 1, we obtain $\tilde{\mu}(298\,\text{K}) = 1.7979\times10^{-5}GPa^{-1}day^{-1}$. Taking *M*=1250 (which for δ=3 nm gives R=4.75 microns), *T=298 K*, and fitting Eq. (12) to any of two points from Table 1, we obtain $T_0 = 525.095K$.

There are two possible reasons why T_0 is slightly lower than the annealing temperature 573 K: (1) stress relaxation during annealing was not complete; or, (2) it was complete but new internal stresses that appeared during cooling partially relaxed during cooling. Since flame speed in [14] was increased in accordance with theoretical predictions even after annealing within 10 minutes at 378 K (i.e., almost complete stress relaxation occurred), then complete stress relaxation definitely should occur at 573 K during 15 minutes of annealing (see Figs. 4 and 5 and

Table 2). Thus, *partial relaxation of stresses took place during cooling, i.e., suggesting that increasing the cooling rate is desirable.*

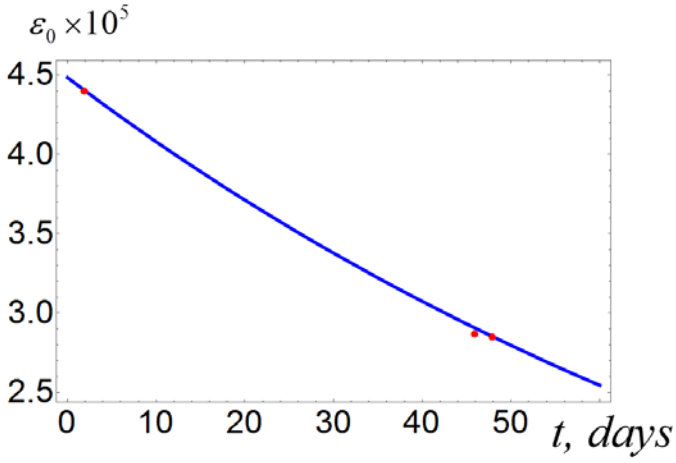

Fig. 4 Relaxation of the dilatational strain in Al core during storage at 298 K and $T_0 = 525.095K$. Curve corresponds to Eq. (12); experimental points for 2 and 48 days are from the current work; experimental point for 46 days is from [15]. Plot for relaxation of the magnitude of the hoop stresses can be obtained by rescaling this and all figures below by a factor of $MK_1 / 2 = 47500GPa$.

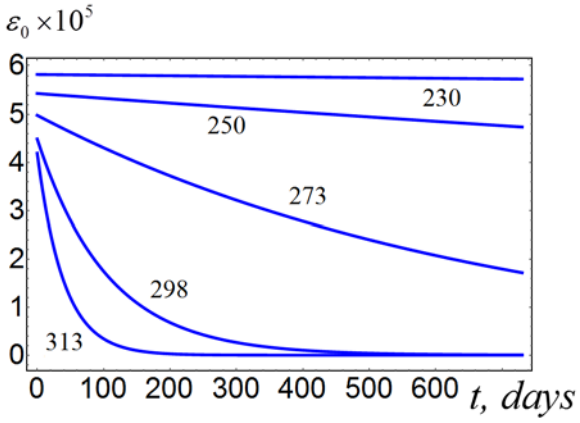

Fig. 5. Calculated relaxation of the dilatational strain in Al core during storage at different ambient temperatures shown near the curves in Kelvin for $T_0 = 525.095K$.

Theoretical plot for the relaxation of the dilatational strain in Al core during storage at 298 K and $T_0 = 525.095K$ is shown in Fig. 4 along with experimental data from the current work and [15]. Note that corresponding values of the hoop stresses and plots for their relaxation of can be obtained by multiplying dilatational strain ε_0 by a factor of $-MK_1/2 = -47500GPa$. In particular, measured dilatational strains of 4.40×10^{-5} and 2.85×10^{-5} after 2 and 48 days of storage cause compressive hoop stresses in the shell of 2.09 GPa and 1.35 GPa, respectively.

To roughly estimate temperature dependence of the creep and stress relaxation, we assume annealing at 378 K for 10 minutes (which was performed in [14] and led to the theoretically predicted flame propagation speed) the internal stresses relaxed by 90%. Substituting these numbers into Eq. (10), we obtain $\tilde{\mu}(378\,\mathrm{K}) = 0.6314 GPa^{-1}day^{-1}$.

Substituting $\tilde{\mu}(298\,\mathrm{K})$ and $\tilde{\mu}(378\,\mathrm{K})$ in the last Eq. (2), we determine the activation energy $Q = 2.03377\times10^{-19}\,J$ and pre-exponential multiplier $\bar{\mu} = 5.4027\times10^{16} GPa^{-1}day^{-1}$. All material parameters are reported in Table 2.

Table 2. Material parameters for aluminum (subscript 1) and alumina (subscript 2) at room temperature [15], as well as estimated parameters for creep in alumina.

K_1 (GPa)	K_2 (GPa)	G_2 (GPa)	α_1 (10^5 K^{-1})	α_2 (10^5 K^{-1})
76	252	163	2.33	0.54
T_0(K)	$\tilde{\mu}$ @ 298 K ($10^5\ GPa^{-1}day^{-1}$)	$\tilde{\mu}$ @ 378 K ($GPa^{-1}day^{-1}$)	$\bar{\mu}$ ($10^{-16} GPa^{-1}day^{-1}$)	Q ($10^{19}\,J$)
525.095	1.7979	0.6314	5.4027	2.03377

III.4. Modeling of dilatational strain relaxation during storage and annealing of Al particles

Equation (12) and the last Eq. (2) will be used with parameters from Table 2, $T_0 = 525.095K$, and M=1250. Figure 5 illustrates how dilatational strain relaxes within two years of particle storage at different ambient temperatures. Keeping the powder stored in low ambient temperature slows the relaxation rate of pre-stressed powder. Figure 5 shows that lower ambient temperature allows the large initial value of the dilatational strain from pre-stressed particles to exhibit slower relaxation rates. Thus, keeping particles at 273 K instead of f 298 K significantly suppresses stress relaxation, especially during the first year. At 230 K stress relaxation is negligible and at 250 K it is very small. At the same time, increasing the storage temperature up to 313 K essentially accelerates stress relaxation in comparison with 298 K, especially within first 100 days.

We can now apply Eq. (11) to model annealing process at different temperatures with $T_0 = 298K$ (Fig. 6). For simplicity, we neglect stress relaxation during heating. After heating to annealing temperature, compressive volumetric strain in the core (and corresponding tensile stresses in a shell) is completely determined by the annealing temperature (see Eq. (11) at t=0). While annealing to 398 K, 90% of the stresses relax in 10 minutes (Fig. 6a), and this case was assumed for determination of the activation energy Q. With such a Q, full relaxation of the internal stresses occurs at 473 K and 573 K during 1 *s* and 0.004 *s*, respectively. Due to approximated character of determination of Q and its strong effect on the results, we are not claiming quantitative prediction here. However, qualitatively, it is now clear that if annealing at 398 K during 10 minutes increases the flame rate according to the theory, i.e., these parameters

are sufficient for almost complete stress relaxation, then annealing time at higher temperatures should be much shorter. This also will reduce probability of sintering of particles, which may lead to local stress concentration in a shell and suppress MDM [20]. The main focus of the experimental research will be on more precise determination of the creep parameters in the temperature range, determination of the minimum required annealing time and cooling rate in order to avoid stress relaxation during cooling.

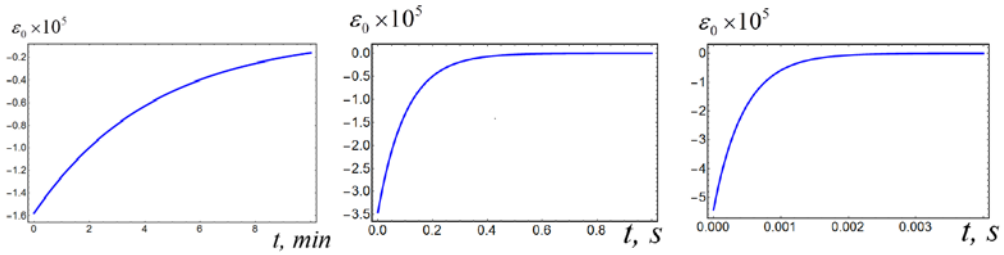

(a) (b) (c)

Fig. 6. Calculated relaxation of the volumetric strain in Al core for $T_0 = 298K$ during annealing at 378 K (a), 473 K (b), and 573 K (c).

IV. CONCLUDING REMARKS

This work represents a next step in improving reactivity of micron-scale Al core-alumina shell particles for energetic applications. The key experimental result consists of measurement of the dilatational volumetric strain in the Al core, utilizing x-ray diffraction with synchrotron radiation, after 2 and 48 days of storage after pre-stressing by heat treatment. Theoretical analysis developed here is the first demonstration of creep and stress relaxation in few nm thick alumina shell at room temperature. The measured dilatational strains in a core of 4.40×10^{-5} and

2.85×10^{-5} after 2 and 48 days of storage cause compressive hoop stresses in alumina shell of 2.09 GPa and 1.35 GPa, respectively. It was shown that the flame propagation rate after such a treatment increases for Al+CuO mixture by 37% and 25%, respectively, in comparison with untreated particles. This is qualitatively consistent with the theoretical predictions in [5,6] that compressive stresses in the shell (and, consequently, tensile mean stress in the core) increases the flame speed. These results show larger stresses correlate to larger increases in flame speed.

Simple analytical model for creep in alumna and stress relaxation in Al core-alumina shell structure is developed. Based on available experiments, an activation energy and pre-exponential multiplier are estimated. Then theoretical modeling of creep in some regimes was performed, which lead to some important conclusions and practical recommendations. Thus, it was concluded that complete stress relaxation occurs for annealing at 573 K during 15 minutes; however, partial relaxation of stresses took place during cooling. Thus, increasing in the cooling rate is desirable for reduction of undesirable internal stress relaxation. Figure 5 gives information about the environmental temperature and time particles can be stored without significant relaxation of internal stresses. Figure 6 allows one to estimate the required time for complete relaxation of internal stresses during annealing at different temperatures. While more experimental data will definitely lead to more precise values of material parameters and change the obtained numbers, we do not expect that our qualitative conclusions will be changed. The obtained experimental and theoretical results represent important progress in our main objective of designing optimal Al micron-scale particles for energy-related applications. Also, this new model for stress relaxation in an alumina shell can be used for improving the model for melting of Al particles covered by an alumina shell [21] and interpreting of experimental data.

ACKNOWLEDGEMENTS

The authors gratefully acknowledge the support from ONR N00014-16-1-2079 managed by Dr. C. Bedford. The Advanced Light Source is supported by the Director, Office of Science, Office of Basic Energy Sciences, Materials Sciences Division, of the U.S. Department of Energy under Contract No. DE-AC02-05CH11231 at Lawrence Berkeley National Laboratory and University of California, Berkeley, California.

References

[1] V. Rosenband, Combust. Flame 137 (2004) 366.

[2] D.A. Firmansyah, K. Sullivan, K.S. Lee, Y.H. Kim, R. Zahaf, M.R. Zachariah, and D. Lee, J. Phys. Chem. C 116 (2012) 404.

[3] S. Chowdhury, K. Sullivan, N. Piekiel, L. Zhou, and M. R. Zachariah, J. Phys. Chem. C 114 (2010) 9191.

[4] Egan, G. C.; LaGrange, T.; Zachariah, M. R. *J. Phys. Chem. C* **2015**, 119, 2792−2797.

[5] V. I. Levitas, B. W. Asay, S. F. Son, and M. Pantoya, J. Appl. Phys. 101 (2007) 083524.

[6] V. I. Levitas, Phil. Trans. R. Soc. A 371 (2013) 20120215.

[7] V. I. Levitas, M. L. Pantoya, and B. Dikici, Appl. Phys. Lett. 92 (2008) 011921.

[8] B. S. Bockmon, M. L. Pantoya, S. F. Son, B. W. Asay, and J. T. Mang, J. Appl. Phys. 98 (2005) 064903.

[9] V. E. Sanders, B. W. Asay, T. J. Foley, B. C. Tappan, A. N. Pacheco, and S.F. Son, J. Propul. Power 23 (2007) 707.

[10] V. I. Levitas, M. L. Pantoya, K. W. Watson, Appl. Phys. Lett. 92 (2008) 201917.

[11] V. I. Levitas, M. L. Pantoya, S. Dean, Combust. Flame 161 (2014) 1668.

[12] Y. Ohkura, P. M. Rao, and X. Zheng, Combust. Flame 158 (2011) 2544.

[13] V. I. Levitas, B. Dikici, M. L. Pantoya, Combust. Flame 158 (2011) 1413.

[14] V. I. Levitas, J. McCollum, and M. L. Pantoya, Scientific Reports, 5 (2015) 7879.

[15] Levitas, V.I., McCollum, J., Pantoya, M.L., and Tamura N. J. Appl. Phys., 2015, 118, 094305.

[16] J. McCollum, M.L. Pantoya, N. Tamura, Improving Aluminum Particle Reactivity by Annealing and Quenching Treatments: Synchrotron X-ray Diffraction Analysis of Strain, Acta Mater. In Press (2015).

[17] M. Kunz, N. Tamura, K. Chen, A.A. MacDowell, R.S. Celestre, M.M. Church, et al., A dedicated superbend X-ray microdiffraction beamline for materials, geo-, and environmental sciences at the advanced light source., Rev. Sci. Instrum. 80 (2009) 035108.

[18] N. Tamura, XMAS: a versatile tool for analyzing syncrotron x-ray microdiffraction data. Microdiffraction analysis local and near surface hierarchical organization of defects, London, 2013.

[19] K.S. Kappagantula, M.L. Pantoya, J. Horn, Effect of surface coatings on aluminum fuel particles toward nanocomposite combustion, Surf. Coatings Technol. 237 (2013) 456–459. doi:10.1016/j.surfcoat.2013.08.035.

[20] Levitas V.I. and Hwang Y.S. J. Appl. Phys., 2016, in press.

[21] V.I. Levitas, M. L. Pantoya, G. Chauhan, I. Rivero, J. Phys. Chem. C 113 (2009) 14088.